Polymerization of Ethylene in the Gas Phase - A new combined hardware and software tool

Yashmin Blazzio, Sebastien Norsic, Nida Sheibat-Othman, Timothy Mckenna

Polymerization of Ethylene in the Gas Phase – A new combined hardware and software tool

Yashmin R. Blazzio[a], Sebastien Norsic[a], Nida Sheibat-Othman[b], Timothy F.L. McKenna[a,*]

[a] C2P2-UMR 5265, Université de Lyon, CNRS, CPE Lyon, Université Claude Bernard Lyon 1, 69616 Villeurbanne Cedex, France
[b] University of Lyon, Université Claude Bernard Lyon 1, CNRS, LAGEPP-UMR 5007, 69622 Villeurbanne Cedex, France

*timothy.mckenna@univ-lyon1.fr

Abstract

A multi-reactor stopped-flow apparatus has been developed to study gas-phase olefin polymerization at short times under industrially meaningful reaction conditions. A simplified single phase 1D dynamic model of the reactor was used to develop an estimator of the polymerization rate from the recorded measurements of temperature, pressure, and flow rates. This combined hardware/software tool was used to investigate the difference between two commercial catalysts that showed different activity profiles in a standard laboratory reactor. Using the temperature and rate profiles generated with this new reactor it was shown that one of the catalysts exhibited extremely rapid light off, and an associated initial temperature spike. Since the observed activity of this catalyst was much lower than that of the other catalyst in the lab scale reactor, it is postulated that thermal deactivation, which cannot be detected in the larger system, was responsible for the lower long term activities.

1 Introduction

Polyolefins are an integral part of our daily lives, with over 100 million tons of polyethylene (PE) alone produced yearly. A wide range of material properties can be obtained from different manufacturing processes and polymerization catalysts, each adapted to specific applications and commercial needs. Gas phase ethylene processes were the last commercial processes to be developed, but now account for a good fraction of the global production of linear low density polyethylene (LLDPE), and of high density polyethylene (HDPE) in swing processes.

Nevertheless, heat removal in gas-phase reactors is more critical than in solution and slurry, given the poor heat transfer properties of the gaseous medium. Temperature excursions in the growing particles can cause the reactor to overheat, and can compromise the quality of the

produced polymer as several properties (e.g. molecular weight, chemical composition and catalyst kinetic behavior) are dependent on the reaction temperature at the catalytic sites. Additionally, particle softening and agglomeration can cause operational problems such as formation of sheets in the reactor walls, resulting in ineffective operation of reactor components, such as the fluidization of the bed.[1–3] Paradoxically, producers need to run their reactors at the highest allowable temperature in order to maintain high rates of production. This can obviously create dangerous situations, especially on small fresh catalyst particles. It has been demonstrated extensively that resistance to heat transfer is greatest for small particles during the very early stages of polymerization, i.e. freshly injected catalyst or prepolymer.[4–6]

This nascent phase of the polymerization can be thought of as the initial tens of seconds of the lifetime of the catalyst particle in the reactor. This period is crucial in ensuring satisfactory properties of the final polymer as several very important steps occur rapidly and simultaneously:

- catalyst activation takes place;
- polymer build-up causes the catalyst particle to fragment and transform into a growing polymer particle;
- physical stress during fragmentation and rapid expansion help to define particle morphology;
- polymer physical properties evolve rapidly (this defines transport rates and influences how the stresses are dissipated).

The rapid changes that take place here depend on many factors, including the rate of polymerization, the instantaneous properties of the polymer being formed, the local composition and temperature of the continuous phase, and the morphology and physical properties of the catalyst support.[7–9] The length (10-100 microns) and time (fractions of a second to seconds) scales over which the phenomena of interest occur make their experimental investigation very challenging in standard equipment, and as we have explained in the past it is desirable to have specially designed reactors for this purpose, and stopped flow techniques appear to be quite promising for this type of application.[10] At the risk of over-simplifying, the stopped-flow technique consists of rapidly mixing the reactant components so the reaction will take place in a well-defined environment for a specific time.

Subsequently, the reaction is quickly and precisely quenched by changing the reaction environment.

Different groups have studied stopped-flow reactors for slurry polymerizations (i.e. with a continuous liquid phase), and showed that this general approach can be used to mimic polymerization in conditions similar to those found in commercial processes, and can provide valuable information about the earliest stages of reaction.[10–17] However, it is important to point out that we expect significant differences at this point in the process between gas phase and slurry polymerizations. Therefore, given the very different process constraints (phases, flow rates, heat transfer characteristics), a specific technology needs to be developed for gas phase polymerization processes.

The main challenge in studying gas-phase polymerization reactions at early stages is to mimic the conditions found in industrial reactors, and in particular the heat transfer conditions that are governed by the relative gas-particle velocities and can be strongly influenced by the composition of the gas phase. For that, it would be necessary to expose the catalyst particles to several different process gases, at moderate pressures and different relative gas-particle velocities. Clearly, making a miniaturized fluidized bed reactor (FBR) is neither practical nor representative of a larger scale device given that the reaction hydrodynamics are scale-dependent.

One promising manner of applying the stopped-flow technique in gas phase polymerizations is to cause monomer to flow over a fixed bed of dispersant and catalyst for a defined period of time, then abruptly stop the reactant flow and instantaneously quench the reaction by changing the reaction environment by, for example, applying the flow of a quenching gas such as CO_2. While this is clearly not what happens in a lab or industrial scale reactors, the essential component of the experiment is to expose the particles to both reasonable reaction *and* heat transfer conditions.

Previous work from our research group has shown that this approach has potential for gas phase processes.[6,18,19] The first stopped-flow reactor adapted to gas-phase olefin polymerization consisted of a fixed bed having a tubular shape (into which the catalyst/dispersant mix was packed).[18] This proved to be a useful tool for studying morphology, fragmentation and reaction kinetics on supported catalysts for reaction durations as short as 100 ms. However, the set-up did not allow for controlled flow rates and presented difficulties associated with back flow at low pressures and temperature gradients in the

reaction bed. This eventually prompted a redesign of the reactor with a shallower, disc-shaped fixed bed intended to help reduce temperature gradients in the reactor.[6] This version included solenoid valves for accurate feed rates, as well as a reduced aspect ratio (a cylinder of d = 0.5 cm and L = 1 cm) that aimed to lower the temperature gradients in the reaction bed. The reactor consisted of a metal chamber closed with a fritted metal cartridge with thermocouples at the entry and exit of the reactor that allowed to measure the inlet and outlet gas temperatures. However, a detailed modelling study later showed that despite the redesign, there was a possibility of encountering non-negligible temperature gradients inside the reactor despite its small volume.[20,21] Finally, this set-up was not adapted to inject components that are liquid at room temperature (e.g. comonomers and alkanes used in condensed mode operation).

Despite these limitations, it was possible to learn much about the nascent phase of gas phase polymerizations. For instance, the energy balance model showed that even under controlled heat transfer conditions, the particle temperature could increase by 15-20 °C in 2 to 5 seconds, sometimes reaching values responsible for polymer melting for low gas velocities.[18] Also, by following thermal properties of the polymers, Tioni et al.[22] observed an effect of constrained crystal growth in the pores of a silica-supported metallocene at increasing reaction times, leading to a suppression of the crystallization temperature. The use of differential scanning calorimetry thus allowed to see the nano and meso pores of the silica 'disappear' as a function of time during the initial stages of reaction, thus providing a time frame for the particle fragmentation. This implies that it would be interesting to use this type of analysis as one additional tool for understanding catalyst activation and morphology development.

For all of these reasons, we decided to redesign and build a more robust stopped flow reaction tool to study gas phase polymerization to overcome said limitations, and to improve "user-friendliness" and enhance the information extracted from the experiment. This includes both the reactor system (hardware) and a state estimation tool (software) that allows one to estimate reaction rates and temperatures for the duration of an experiment, not just the end.

2 Experimental

2.1 Materials and preparation

Nitrogen gas (99.999% purity) and carbon dioxide (99.995% purity) from Air Liquide France were used as received. Ethylene (99.95% purity) was purchased from Air Liquide France and

purified by flowing it through three purification columns: The first was filled with reduced BASF R3-16 catalyst (CuO supported on alumina), the second with molecular sieves (13X, 3A, Sigma-Aldrich), and finally a column of Selexsorb COS (Alcoa).

Three catalysts were used in this work: a Ziegler-Natta catalyst (ZN), a Zirconocene catalyst, hereafter referred to as CpZ, and a commercial constrained geometry metallocene catalyst (particles assumed spherical with average diameter of 40 µm), hereafter referred to as CGC. All catalysts were supplied by industrial partners, so no information about composition can be supplied, but we will be able to estimate their activity.

2.2 Polymerizations

2.2.1 Standard polymerizations

Standard polymerization reactions were carried out in a spherical 2.5 L lab-scale semi-batch reactor using CpZ and CGC. The system was cleaned before use with heptane and kept under isothermal conditions, with vacuum/argon cycles to purge the reactor prior to the polymerization reaction. An injection cartridge containing catalyst and seedbed was prepared inside a Glove Box under an argon atmosphere. 100 g of sodium chloride (NaCl), dried under vacuum at 400 °C for 4 hours, was used as seed bed. A desired amount of alkylating agents was introduced in the reactor prior to catalyst injection. Catalysts were injected under monomer pressure, and the moment of injection marked the beginning of the polymerization reaction. Mechanical agitation was kept constant during the reaction at 200 rpm. The experiments were performed for 60 minutes.

For the CpZ used in this study, 50 mg catalyst were employed. As scavenger for the reactor environment, 0.8 mL of a 1 M solution of Triisobutylaluminum (TIBA) were used. The reactions were performed in homopolymerization with ethylene under constant pressure of 7.5 bar and reaction temperature of 84 °C.

For the constrained geometry catalyst used in this study (CGC), 100 mg catalyst were employed. 0.5 mL of a 1 M solution of TIBA were used as the scavenger for the reactor environment. The reactions were performed in homopolymerization with Ethylene under constant pressure of 7.5 bar and reaction temperature of 70 °C.

A pressure reducer was used to maintain the pressure in the spherical reactor constant throughout the reaction. Continuous measurements of the monomer pressure in the ballast were interpreted using the Soave-Redlich-Kwong equation of state (SRK-EOS)[23], to

calculate the productivity. Finally, the derivative of the pressure drop provided an estimate of the reaction rate.

The polymerization was quenched at the desired time by simultaneously venting the monomer and cooling the reactor to room temperature. The formed polymer powder was then washed in water to remove the NaCl seedbed and, finally, dried under vacuum at 70 °C for at least two hours.

2.2.2 Stopped flow polymerization

The ZN catalyst was pre-activated in the glovebox with a 1 M triethyl aluminum (TEA) solution in dry heptane. The desired amount of the TEA solution is added to the salt/catalyst mixture, aiming for a specific Al/metal ratio. The mixture is vigorously agitated by hand, then dried under active vacuum for at least 15 minutes before use.

All 3 catalysts were used in the stopped flow reactor. Three stopped flow reactors are used in the current work, the original cylindrical disc-shaped reactor (CR) described in reference[6], and 2 newly designed annular reactors that are described in more detail below. The annular stopped flow reactor prototype (ASFRp) and the annular stopped flow reactor (ASFR) are similar in concept, and in the ways in which they are sealed and attached to the rest of the reactor set-up, differing only in their dimensions (see Figure 1 below).

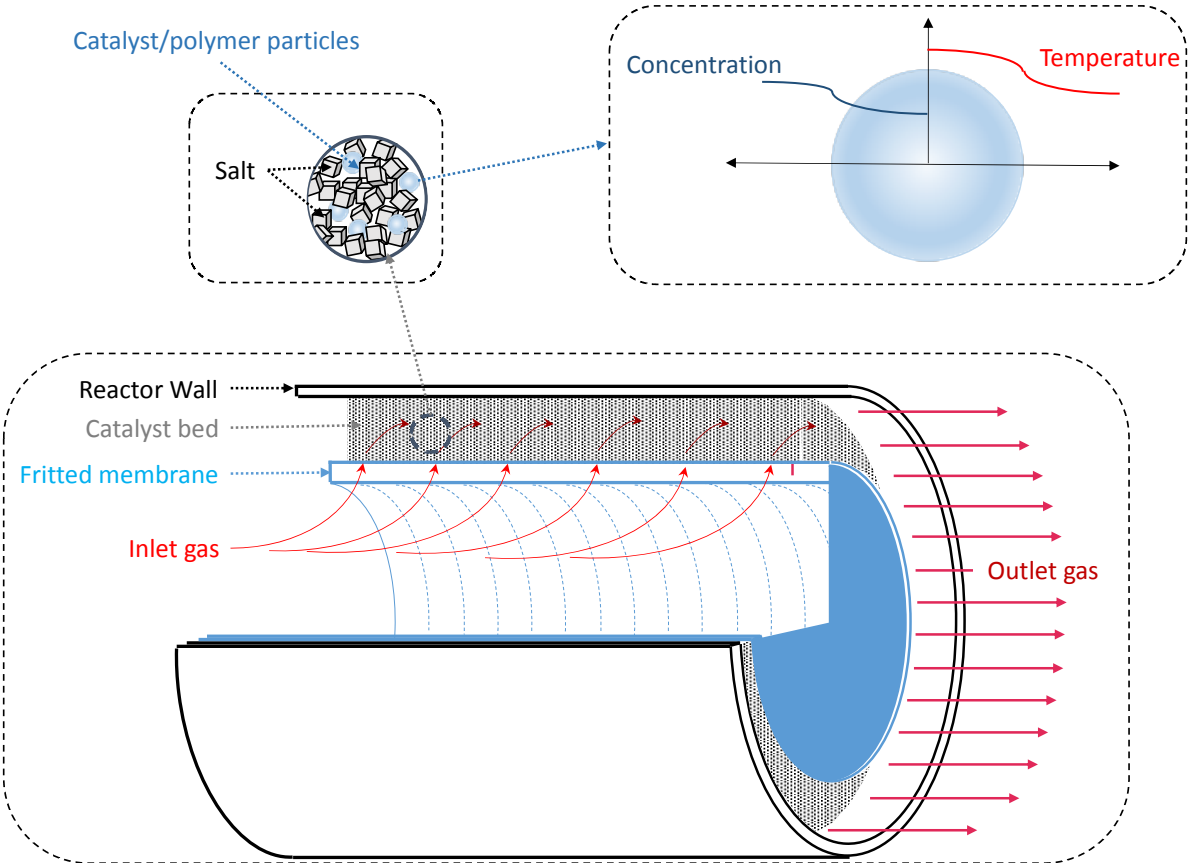

Figure 1. Annular stopped flow reactor (ASFR) concept. The gas enters the open end of the interior of the cylinder (sealed at the opposite end), passes through the pores of the filter, then through the fixed bed of catalyst and salt present in the cylinder periphery, and exits through the opposite end of the annular space.

Regardless of the version of the stopped flow reactor employed, the reactor preparation methods and polymerization procedure remain the same, as in reference[6]. The reaction medium is composed of a solid mixture of catalyst and fine salt as inert seedbed (5 µm crystals agglomerated into particles of average diameter of 50 µm) at 2-5 % by weight of catalyst with respect to the total mass of salt. The solid mixture is kept in place, in the reactor gap, by a metal frit for the original cylindrical reactor, or by layer of dry glass wool (approximately 500 mg) for the annular reactors ASFRp and ASFR. The reactors are packed and sealed inside a glove box under Argon atmosphere.

The reactors are then heated, either by submerging them in a water bath in the case of the cylindrical reactor and the ASFRp, or in the case of the ASFR, in a heating chamber under nitrogen flow. All reactors are pressurized with nitrogen for 20 s to avoid compression heat effects when initiating the monomer flow (It was observed by Browning et al.[20,21] that if the pressure in a small reactor was instantaneously increased from 1 to 7 bars, the temperature of the gas in the reactor increased). The polymerization is launched by opening the monomer

flow to the system once thermal equilibrium has been reached. Immediately after the desired polymerization time is completed, the reactor is flushed with a shot of carbon dioxide for 15 s, to kill the catalysts in such a way that we can recover the particles intact. At last, the reactor is purged with nitrogen flow for 15 s. The polymer production is monitored gravimetrically by weighing the reactors before and after the reaction in a balance with 10 mg precision. The data collected for each experiment includes: the mass of catalyst and salt, the mass of glass wool (for energy balance calculations), the final polymer yield, the oven/bath temperature, the duration of the reaction, the inlet gas mass flow rates and pressures, and the inlet and outlet gas temperatures. Unless otherwise mentioned, the average gas velocity was maintained at 55 cm/s for all experiments to mimic fluidized bed reactor conditions.

An orthogonal factorial design of experiments (DOE) approach was used to study the impact of process parameters on the kinetics and properties of nascent polymers made with catalysts CpZ and CGC.[24] The responses (dependent variables) for the experimental evaluation were the molecular weight, polymer crystallinity and melting temperature (T_{m}).

For catalyst CpZ, the variable (independent) factors were the reaction time and comonomer (1-hexene) content in the gas feed. The experiments were performed in random order, and the ethylene pressure (7.5 bar) and reactor temperature (84 °C) were kept constant for all experimental runs. For this catalyst, the full factorial composition of two factors varying at three levels (3^2 factorial design) results in a total of 9 experiments.

For catalyst CGC, the varying factors were the reaction time, the comonomer (1-hexene) content in the gas feed and the hydrogen content in the gas feed. The experiments were performed in random order and the ethylene pressure (7.5 bar) and reactor temperature (70 °C) were kept constant for all experimental runs. For this catalyst, the full factorial composition of three factors varying at three levels (3^3 factorial design) results in a total of 27 experiments. In this case, we opted for a fractional factorial design where experiments in which two of the varying conditions are of the same level were excluded from the analysis, thus resulting in 9 experiments.

Three repetitions of the experiment on the central point (0, 0, 0) were performed for each catalyst to estimate the experimental error. Extra points were also added. The experimental limits for the independent variables were defined based on indications from the catalyst suppliers. The chosen factors and levels of variation can be found in Tables 1 and 2.

Table 1. Factors and levels of variation for catalyst CpZ

Variable factor		Level			
		-1	0	1	Extra
		Low	Middle	High	
X_1	[1-C_6] (wt %)	0	8	16	20
X_2	Time (s)	5	30	55	---

Table 2. Factors and levels of variation for catalyst CGC

Variable factor		Level			
		-1	0	1	Extra
		Low	Middle	High	
X_1	[H_2] (mol %)	0	0.3	0.6	1.5
X_3	Time (s)	5	12.5	20	60

2.2.3 Material Characterization

DSC analysis was performed using Mettler Toledo DSC 3+ model. Polyethylene was weighed (typical sample size 5-10 mg) and placed in an aluminum capsule with a volume of 40 uL. The sample was first cooled to – 20 °C, giving start the analysis being heated to 180 °C at a rate of 10 °C/min, held for 10 min and then cooled down to – 20 °C at a rate of 10 °C/min. This temperature was maintained for 10 minutes, and the sample was reheated to 10 °C/min to 180 °C. The melting behavior of the samples was studied in the second heating run from room temperature up to 180 °C at the same rate of cooling to detect the melting point (Tm) and the determination of the melting enthalpy (ΔHf) of the samples. samples. The degree of crystallinity (χc) of the samples was calculated by considering the percentage by weight of the crystalline phase obtained from the polyethylene fraction and the heat of melting from 293 J.g-1 to 100% crystalline polyethylene. The crystallization temperature (Tc) is obtained in the cooling run.

3 Tool Development

3.1 Stopped flow reactor – Hardware component

A review of the literature led us to change the original design in references [6] and [18] from a disc-shaped reactor to a fixed-bed reactor with annular geometry. Several studies with heterogeneous catalysts (not polymerization) showed that this annular design helps to

improve the gas distribution in the reactor and increase the evacuation of the heat generated by the reaction[25–27] and to reduce internal diffusion limitations.[28,29] The concept of this annular stopped flow reactor is shown in Figure 1. Process gases enter the inner portion of sintered metal cylinder that is sealed at the opposite end. They flow through the pores into the packed bed composed of a mixture of salt and catalyst where they react, and exit through the annular space at the end of the reactor.

Before moving to the development of the final reactor configuration, a prototype AFSR (ASFRp) was constructed with the following characteristics:

- Diameters of external cylinder: 22 mm
- Reactor length: 110 mm
- Outer diameter of porous membrane: 17 mm
- Membrane thickness: 2 mm
- Membrane porosity: 43 %
- Pore diameter of membrane: 5 µm

The ASFRp was built with Swagelok 316 stainless-steel male and female VCR locks (Fitting 1/4 in), Swagelok stainless steel VCR 1/4 in. Tube Socket and porous frit were obtained from Stemm (Lyon, FR).

In order to test the concept that the annular reactor design improves the temperature control, a series of tests were run using the ZN catalyst in both the CR of reference [6] and the ASFRp. The resulting outlet temperatures are shown in Figure 2. It can be seen that the difference between the inlet and outlet temperatures is at most 2.5 °C for the ASFRp, whereas it is on the order of 20-35 °C for the CR, despite the higher inlet temperatures for the former. Table 3 shows that the yields from both reactors are similar, demonstrating that the same amount of heat is generated in both polymerization reactors. Clearly the annular geometry offers much more isothermal conditions than the cylindrical disc-shape geometry, and the results appear to be more reproducible. This suggests that we can ignore temperature gradients in the annular reactor length when developing the software tool below (for the catalysts amounts and activities used in this work).

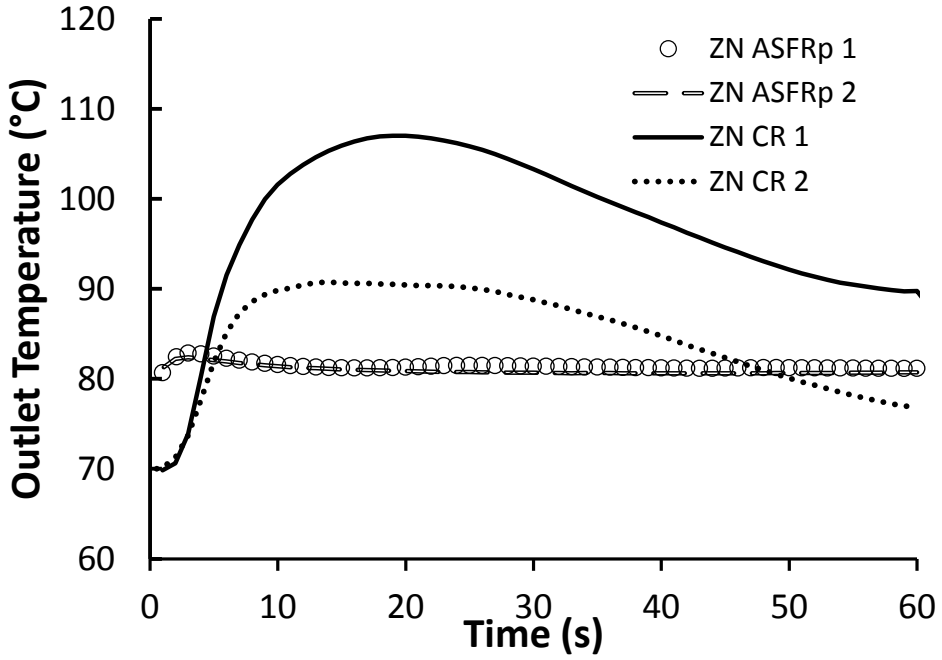

Figure 2. Reactions performed with 30-40 mg ZN catalyst (preactivated with TEA at Al/Ti=60), 7 bars ethylene with gas velocity of 18 cm/s in average. Inlet gas temperatures 70 °C for ZN-CR1 and ZN-CR2, 80 °C for ZN ASFRp1 and ZN ASFRp2. The inlet temperature is 70°C in CR and 80°C in ASFRp.

Table 3. Comparison of yields in the original cylindrical reactor (CR) and the ASFRp prototype for the polymerizations shown in Figure 2.

Experiment #	Yield (g/g)
ZN-CR1	9
ZN-CR2	5
ZN-ASFRp1	6.5
ZN-ASFRp2	8.3

Once the concept of using the annular reactors was validated with the in-house prototype, the entire reactor system was redesigned professionally. The dimensions of the annular reactors were reduced to make them easier to manipulate in the glove box, while providing a bed volume of 6.5 cm^3, which is sufficient to provide enough polymer for analysis, even from short reaction times. The reactors are sealed in the glove box with rubber septa held in place by aluminum crimp caps. The filled reactors can then be easily transported and fitted in place. The feed lines are equipped with needles that pierce the septa but do not allow the exterior

atmosphere to enter the reactor. The same type of porous membrane (with different dimensions) was used in this new construction, and the revised reactor dimensions are as follows:

- Diameters of external cylinder: 16 mm
- Reactor length: 56 mm
- Outer diameter of porous membrane: 10 mm

ASFR can be used three at a time in the structure of the stopped flow reactor (SFR) set-up as shown in Figure 3. There are 3 main zones in this structure:

1. Multiple gas injection lines. The set-up allows feeding multiple gaseous components in the reactor, such as: ethylene or propylene (monomers), hydrogen (chain transfer agent), nitrogen (inert gas) and CO_2 (quenching agent). There is no limit on which components can be used in this section as long as they are not liquids at room temperature. The system operates in pressures between 5 and 16 bar and allows gas velocities as high as 50 cm/s for reaction times as short as 3 seconds. Mass flow meters (from Bronkhorst) control the gas flow rates with the following ranges: 43-2166 g/h for ethylene or propylene, 34-1700 NL/h for nitrogen and CO_2, 4.3-216.6 NL/h for hydrogen;

2. Liquid injection. One liquid component (or one mixture of liquids) can be vaporized then injected into the reactors along with the gaseous components. The liquid vessel is previously filled in the glovebox with the desired liquid or mixture of liquids. The dosed liquids pushed to the evaporator with an overpressure of nitrogen, then vaporized in a three-valve evaporator, and finally carried with the feed gases to the reaction zone. Coriolis mass flow controllers (from Bronkhorst) were also employed for liquid dosing instead of thermal mass flow controllers. This allows a better precision in the flow control and to use any liquid, gas or mixed components without the need of recalibration. Any component that is liquid at room temperature (e.g. n-alkanes or alkenes) can be injected at flow rates between 18.6-930 g/h.

3. Oven with 3 reactors in parallel. The reaction zone consists of three custom-made reactors operated in parallel. The reactors are placed inside an electric heating chamber sealed to ensure good thermal control and equipped with gas detectors that abort the on-going reaction in case of gas leaks.

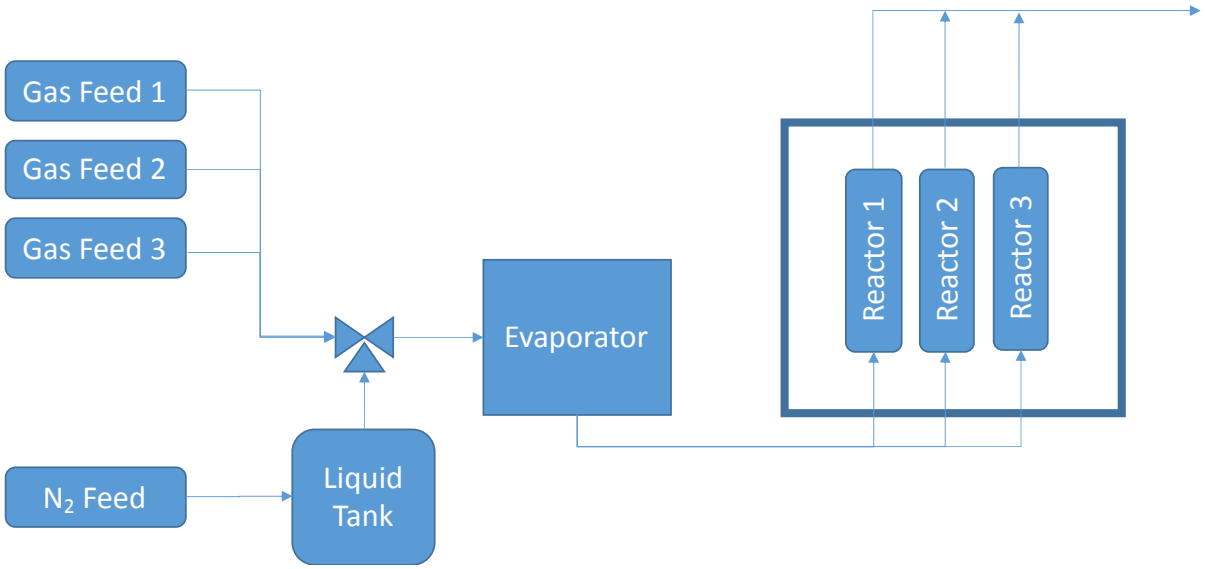

Figure 3: Flow diagram for the ASFR set-up including three reactors in parallel, put into an oven at the desired temperature.

Temperatures of gas at the inlet and outlet of the annular reactor are recorded in intervals of 0.5 s by two 0.5 mm T-type thermocouples placed at the entry and exit of the reactors.

3.2 Development of the high gain observer software tool

In the current study, we treated the reaction zone as single phase and one compartment, which fundamentally means viewing the system as a CSTR. The single phase and single element model is the simplest approach especially due to the lack of experimental data, such as the temperature of the particles or that of gas at different positions. While this is clearly an approximation, as was shown above, it is a reasonable representation given the high flow rates and small dimensions of the reactor. The heat balance is given as follows:

$$mC_p \frac{\mathrm{d}T}{\mathrm{d}t} = F_\mathrm{g}\rho_\mathrm{g}C_{pg}\left(T_\mathrm{g}^\mathrm{in} - T\right) + S_\mathrm{w}h_\mathrm{w}(T_\mathrm{w} - T) + Q_\mathrm{r} \qquad (1)$$

Where mC_p is the product of the mass of the fixed reactor bed and its heat capacity defined in equation (2), F_g, ρ_g and C_{pg} are the mass flow rate, density and heat capacity of the gas, T_g^in and T are the inlet and outlet gas temperatures (gas in the reactor is assumed to be equal to the outlet T), S_w and T_w are the heat transfer surface area and temperature of the walls of the annular space, h_w is the heat transfer coefficient between the gas and the external wall (heat exchange with the wall of the membrane was neglected), and Q_r the total heat of polymerization.

With:

$$mC_p = \varepsilon V \rho_{\mathrm{g}} C_{p_{\mathrm{g}}} + m_s C_{p_{\mathrm{s}}} + m_{\mathrm{glassWool}} C_{p_{\mathrm{glassWool}}} + m_{\mathrm{PE}} C_{p_{\mathrm{PE}}} + m_{\mathrm{c}} C_{p_{\mathrm{c}}} \quad (2)$$

where ε and V are the porosity and volume of the fixed bed, and the subsequent terms are the product of the mass and heat capacity of the salt, glass wool, polymer and catalyst, respectively. The rate of heat generation by the polymerization, Q_{r} is related to R_{p} (kg/s), the rate of polymerization, and ΔH_{p}, the enthalpy of polymerization, as follows:

$$Q_{\mathrm{r}} = R_{\mathrm{p}}\left(-\Delta H_{\mathrm{p}}\right) \quad (3)$$

The heat transfer coefficient at the reactor internal-side wall (h_{w}) is calculated from a combination of both stagnant/ conductive $(h_{\mathrm{w}})_0$ contribution and turbulent/convective $(h_{\mathrm{w}})_{\mathrm{t}}$ contribution, as elucidated by Specchia et al.[30], as follows:

$$h_{\mathrm{w}} = (h_{\mathrm{w}})_0 + (h_{\mathrm{w}})_{\mathrm{t}} \quad (4)$$

The stagnant contribution is obtained from the following relation:[30]

$$\frac{(h_{\mathrm{w}})_0 d_{\mathrm{p}}}{k_{\mathrm{g}}} = 2\varepsilon + \frac{\beta(1-\varepsilon)}{\gamma\frac{k_{\mathrm{g}}}{k_{\mathrm{s}}} + \varphi_{\mathrm{w}}} \quad (5)$$

where φ_{w} is a dimensionless number given by:[30]

$$\varphi_{\mathrm{w}} = 0.0024\left(\frac{d_{\mathrm{R}}}{d_{\mathrm{p}}}\right)^{1.58} \quad (6)$$

with d_{p} the particle diameter (where the salt diameter was used) and d_{R} the bed diameter ($d_{\mathrm{R}} = d_{\mathrm{R}}^{\mathrm{out}} - d_{\mathrm{R}}^{\mathrm{in}}$=5.7 mm). k_{g} and k_{s} represent the thermal conductivity of the monomer gas and salt, respectively. $\gamma = 2/3$ and β=1 in Kunii and Levenspiel [31].

The turbulent contribution $(h_{\mathrm{w}})_{\mathrm{t}}$ is obtained from the following relation, valid for low Reynolds numbers (between 10 and 1200):[30]

$$(h_{\mathrm{w}})_{\mathrm{t}} = \frac{0.0835\, Re^{0.91} k_{\mathrm{g}}}{d_{\mathrm{p}}} \quad (7)$$

The relation was solved for the diameter of the salt particles, given the high dilution of the catalyst particles in the inert seedbed.

With the different measurements and correlations presented above, the only unknown variable in equation 1 is the heat generated by the reaction, that was estimated using an observer.

The reaction rate per catalyst mass, or activity, (g PE/g cat/h) is given by:

$$R_{\mathrm{p,c}} = 3600\frac{R_{\mathrm{p}}}{m_{\mathrm{c}}} \tag{8}$$

Where m_{cat} is the mass of catalyst. The yield is defined by (g PE):

$$Y = \int_0^{t_{\mathrm{f}}} R_{\mathrm{p}}\mathrm{d}t$$

A simple high gain observer was implemented to estimate the reaction rate from the experimental data.[32,33] The method consists of minimizing the relative error between the experimental and the temperature values estimated from the model with a corrective term.[34] The high gain observer of the heat produced by the reaction is given by:

$$\frac{\mathrm{d}\hat{T}}{\mathrm{d}t} = \frac{1}{mC_p}\left(\hat{Q}_{\mathrm{r}} + F_{\mathrm{g}}\rho_{\mathrm{g}}C_{p\mathrm{g}}\left(T_{\mathrm{g}}^{\mathrm{in}} - T\right) + S_{\mathrm{w}}h_{\mathrm{w}}(T_{\mathrm{w}} - T)\right) - 2\theta\left(\hat{T} - T\right) \tag{9}$$

$$\frac{\mathrm{d}\hat{Q}_{\mathrm{r}}}{\mathrm{d}t} = -\theta^2 mC_p\left(\hat{T} - T\right) \tag{10}$$

The corrective term was determined by simulation and fixed at θ =1. The use of an estimator can be comparable to a sliding horizon optimization, where the error between the estimated and real state or parameter is to be minimized over time. Here, it is required to estimate Q_{r} and the error to be minimized is the difference between the estimated and real bed temperatures

The temperature of the reactor wall at the inner surface (T_{w}) was approximated by $T_{\mathrm{w}} = (T_{\mathrm{oven}} + \mathrm{T})/2$, an assumption was made due to lack of experimental measures of the reactor wall.

4 Nascent Gas Phase Polymerization

4.1 HDPE – Temperature effect on CPZ and CGC

Figure 4 shows the polymer mass produced during standard polymerization in the spherical reactor for the two catalysts CpZ and CGC, for 60 minutes reaction. It can be seen that the classic metallocene CpZ presents a slower activation, taking about 35 minutes to reach the maximum polymerization rate, despite the higher gas phase temperature. On the other hand, the CGC catalyst presents very fast activation early in the reaction, reaching the maximum activity at about 5 minutes and then gradually decaying. These profiles would suggest that the

CpZ simply activates more slowly, however short time polymerization rates obtained using the ASFR show a different story, as discussed below.

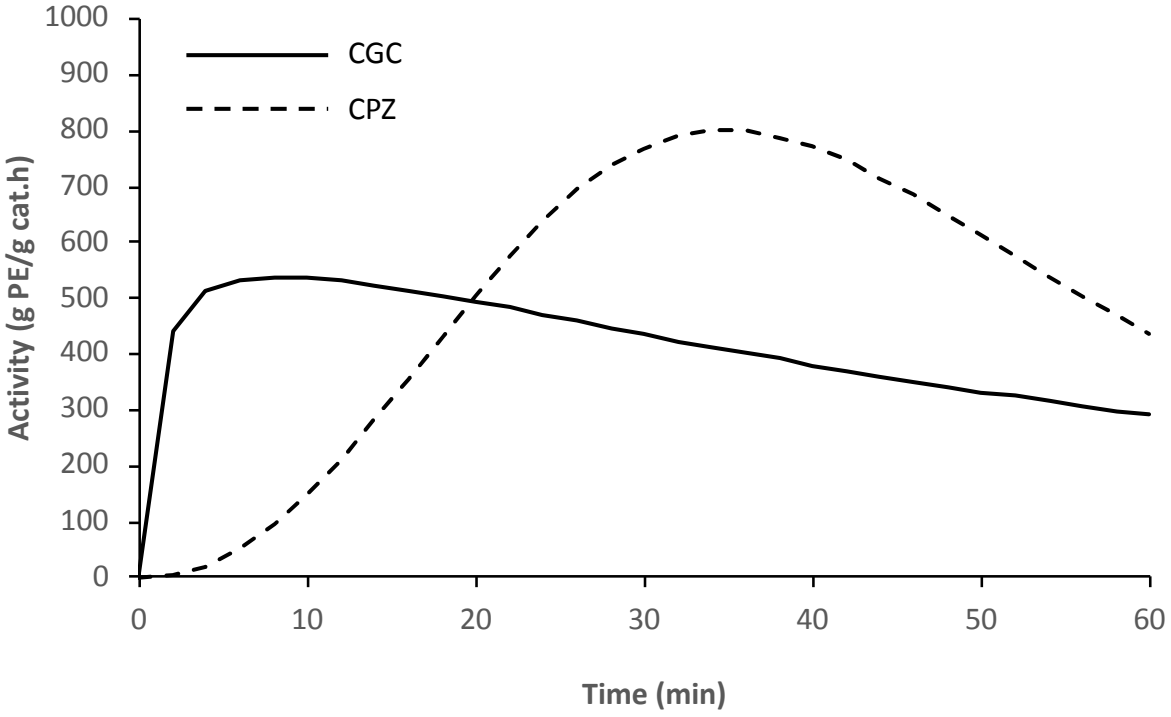

Figure 4: Full polymerization kinetics for 60 minute homopolymerization reactions in the spherical reactor. 7.5 bar of ethylene for both polymerizations. T = 84 °C for CpZ and 70 °C for CGC.

Then, the observer was applied to reactions ranging from 3 to 60 s in the stopped flow reactor, to estimate the catalyst activation at different periods of the nascent phase. Figure 5 shows the estimated polymer mass over time, compared to the experimental result. The error bar is calculated based on the precision of the balance used during weighing (+/- 5 mg). Each curve in the figure consists of an independent experiment, by varying only the duration. The yields estimated using the software tool agree well with the experimentally measured values of polymer mass obtained at the end of each experiment, thereby validating the approach of estimating the reaction rates presented above.

Figure 6 shows the estimated dynamic reaction rates ($R_{p,c}$) for 30 and 60 second runs. The estimated reaction rates for catalyst CGC at short reaction times indicate that the catalyst activates quite quickly (<10 s) and then progresses at a slower activation pace.

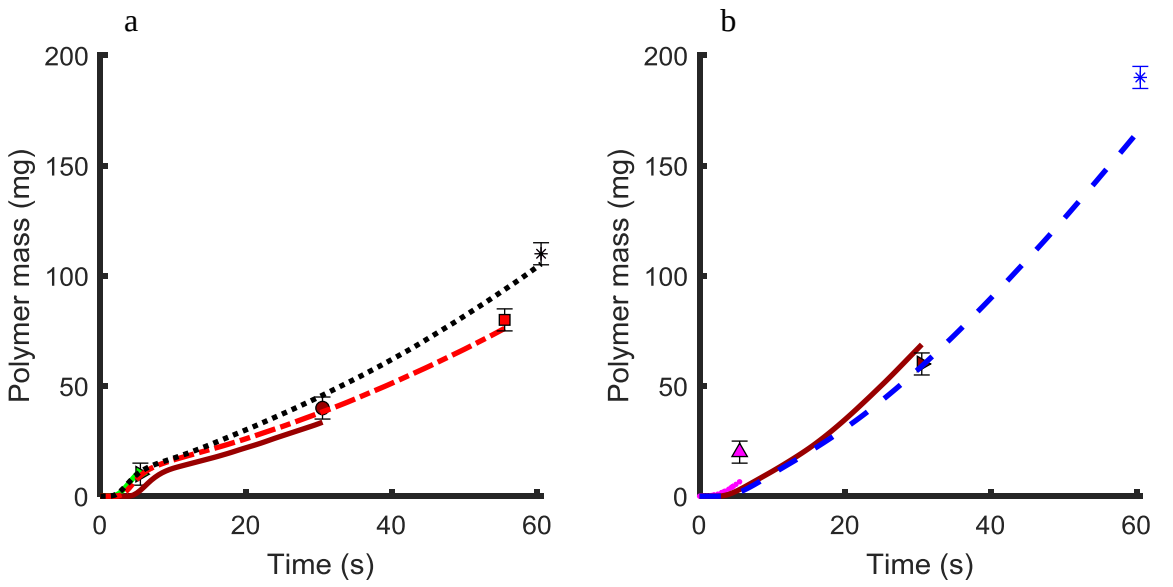

Figure 5: Estimated mass of produced polymer for catalysts: a) CpZ, b) CGC.

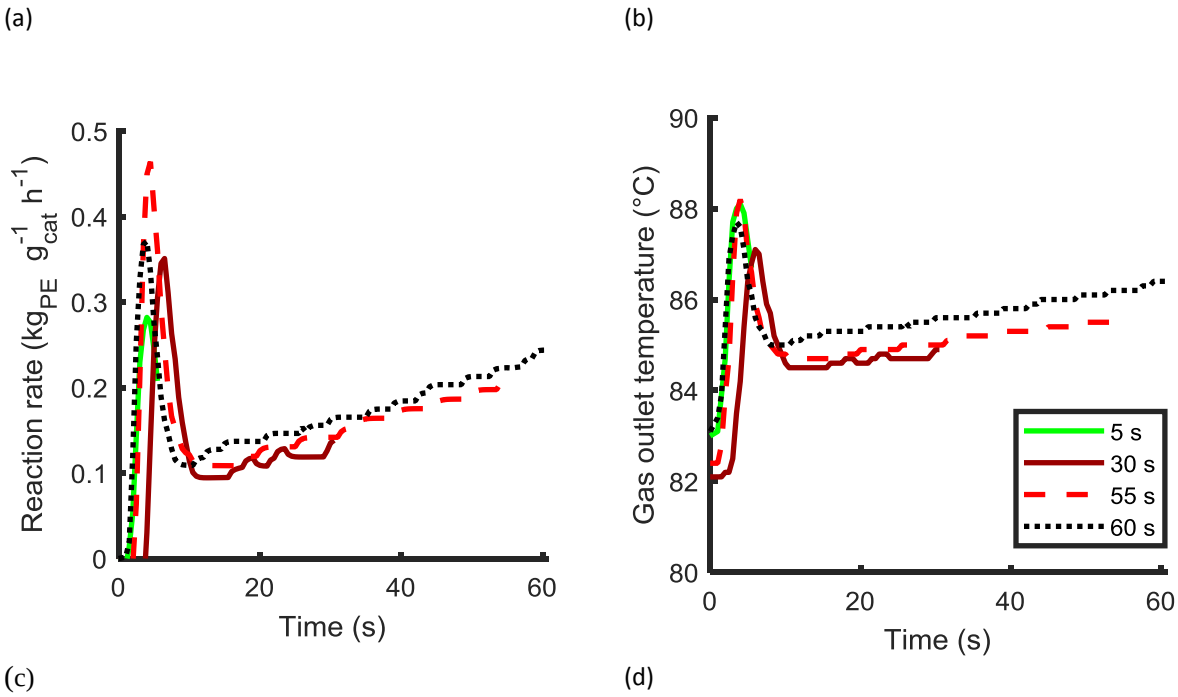

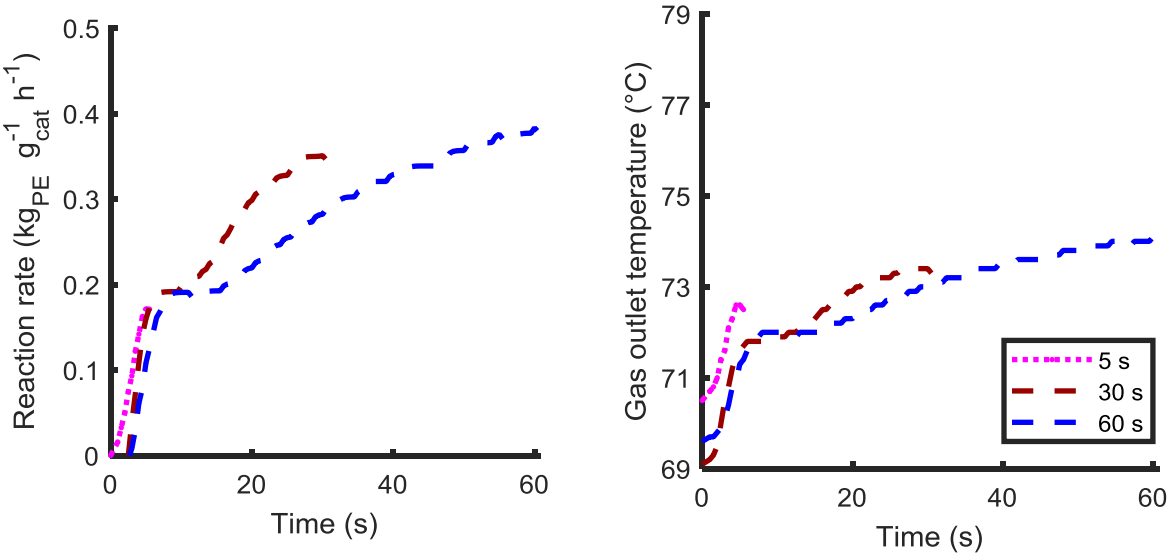

Figure 6: Estimated reaction rates and outlet gas temperatures for catalysts CpZ (a, b) and CGC (c, d).

In Figures 5 and 6, since each curve in the plot derives from an individual experiment, the experimental results are quite reproducible for each of the catalysts. This gives us confidence that the estimated short time polymerization rates are reasonably accurate. If we compare the rate of polymerization and outlet temperatures of the two catalysts, it can be seen that the polymerizations with CpZ showed a pronounced activation peak of 6 degrees in the 5 to 10 seconds, which then subsided and the reaction seemed to progress in a slower increasing rate (that is coherent with the rates shown in Figure 4, if extrapolated). This peak corresponds to a very rapid increase in the gas outlet temperature that can be seen for very short times, which can only be detected in the reactions performed in the stopped-flow reactor. This behavior is contrasted with what is observed for the CGC catalyst, where it can be seen that the initial rise in reaction rate is less significant and does not lead to a sharp increase in the measured outlet temperature. It is possible that the initial light-off with the CpZ is due to the higher initial polymerization temperature but results that cannot be shown here seem to preclude that. This result leads us to postulate that the CpZ catalysts is quite sensitive to temperature (with respect to the CGC), and the slow increase in rate seen in Figure 4 is most likely due to a thermal deactivation of the catalyst CpZ.

4.2 Gas Phase LLDPE – Property evolution

A statistical analysis of the experimental results was performed to investigate the impact of the independent experimental factors (reaction time, 1-hexene content and hydrogen content)

on the melting temperature of the polymer and the crystallinity. It was found that the reaction time and the fraction of 1-hexene in the feed were statistically significant for both catalysts, and that there appeared to be an impact of the hydrogen pressure in the case of the CGC. The response surfaces for the crystallinity are shown in **Erreur ! Source du renvoi introuvable.** for the CpZ catalyst, and for CGC in **Erreur ! Source du renvoi introuvable.**. The impact of 1-hexene on the crystallinity for both catalysts is to be expected for obvious reasons (Figures 7 and 8a respectively). However, it appears to be slightly stronger in the case of the CGC catalyst. According to the catalyst supplier, this catalyst was designed to enhance the incorporation of α-olefin comonomers with respect to conventional metallocenes, and our results confirm this. Similarly, the hydrogen effect is not unexpected as shorter chains generally enhance crystallization (Figure 8b). The fact that no statistically significant result was observed for the CpZ catalyst is because this catalyst produces hydrogen *in situ*, and therefore is less sensitive to small changes in the hydrogen concentration.

a)

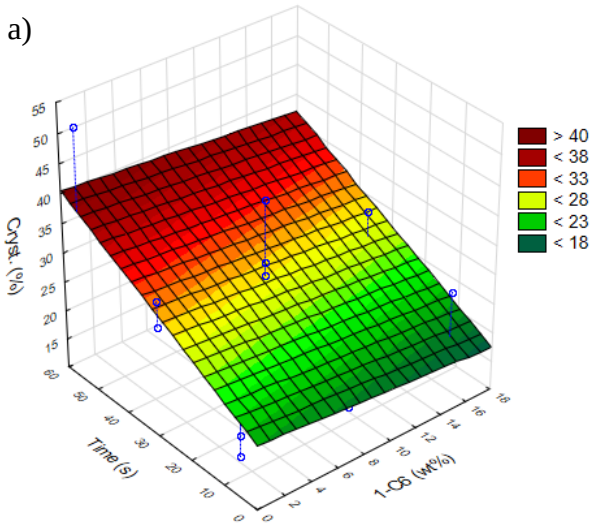

Figure 7: Response surface for polyme However, we added the following description after equation 10 to guide the reader:

r crystallinity using the metallocene CpZ

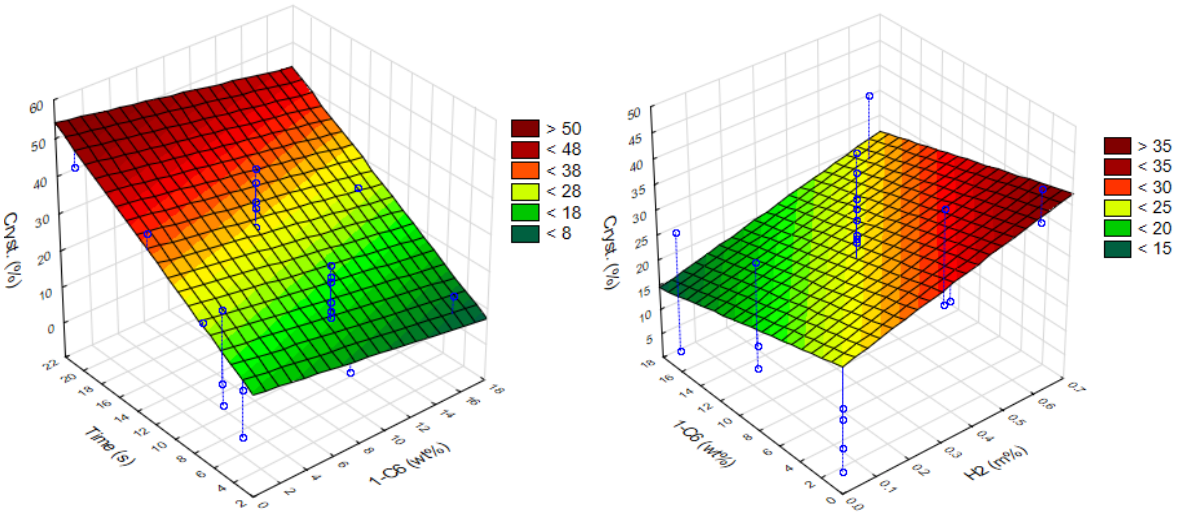

Figure 8: Response surface for polymer crystallinity in terms of 1-hexene content and time (left) and 1-hexene and H_2 content (right) for the CGC catalyst

Perhaps more surprising is the fact that the reaction time is most influential of the process parameters considered (Figure 8a). An apparent temporal dependence of the crystallinity has been observed in previous studies on nascent high density polyethylene in gas phase polymerization on a Ziegler-Natta catalyst, in slurry phase polymerizations using a different Ziegler-Natta catalyst[35], and in gas phase using a silica supported metallocene.[22] The main difference observed in each study is the time scale: the crystallinity increased very quickly with the Ziegler Natta catalysts, taking less than 10 s to reach a constant value.

If we consider the plot in Figure 9, where we see the response surface for the weight average molecular weight (M_w) of the polymer made with CpZ as a function of time and 1-hexene content, we can see that the M_w of the polymer increases with time. This is unexpected as one would expet that this should slow down the crystallization as the longer chains typically crystallize less than shorter ones.

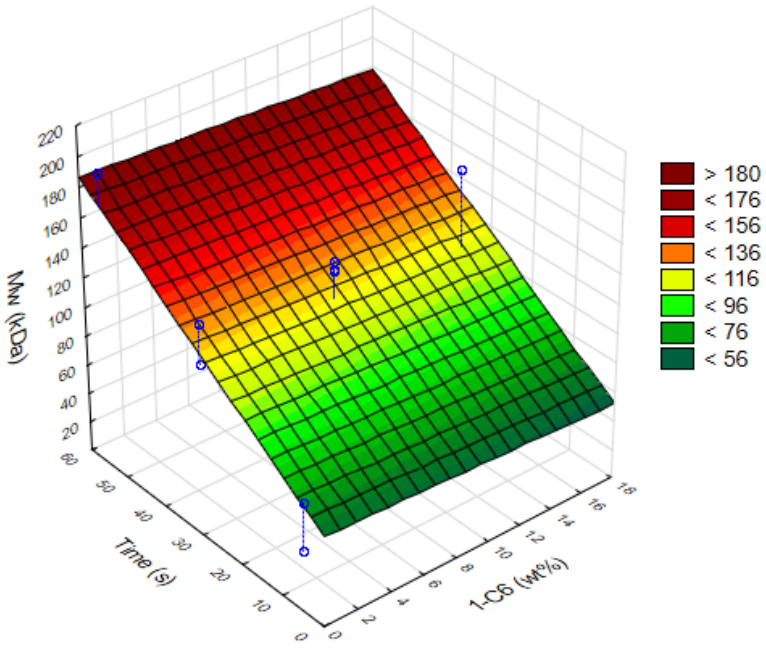

Figure 9: Response surfaces for M_w for classic metallocene CpZ.

The most reasonable explanation for the low polymer crystallinities at early stages of the reaction might is related to the confinement effect of the polymer inside the pores of the support, which is overcome as the reaction progresses and the particle grows.[22] In other words, as shown by Tioni et al.[22] the progression of crystallinity is linked to the fragmentation of the support. When the crystals form in a constrained space (i.e. smaller than that of the equilibrium spherulite size, they are forced to be smaller and thus can form at lower temperatures. Further evidence for this is shown in Figure 10, where we see the evolution of the crystallinity of the homopolymerization of ethylene with CpZ, and in Figure 11, where we see the same evolution for the copolymerization. It can be seen in both figures that the crystallinity of the polymer is very low at short times, and that it also presents a bimodal curve. Furthermore, the crystallization temperature of the peaks at 5 seconds is less than that observed for longer polymerizations. It is also interesting to note that the homopolymer presents a bimodal crystallization peak for longer times than the copolymer. We attribute this to the fact that the copolymerization rate is higher than the homopolymerization rate, so the fragmentation process appears to be completed faster with the former experiment as the amount of polymer accumulated in the pores is higher at the same time for the copolymer. This demonstrates the ability of the tool presented in this paper to do precise studies of fragmentation under realistic conditions.

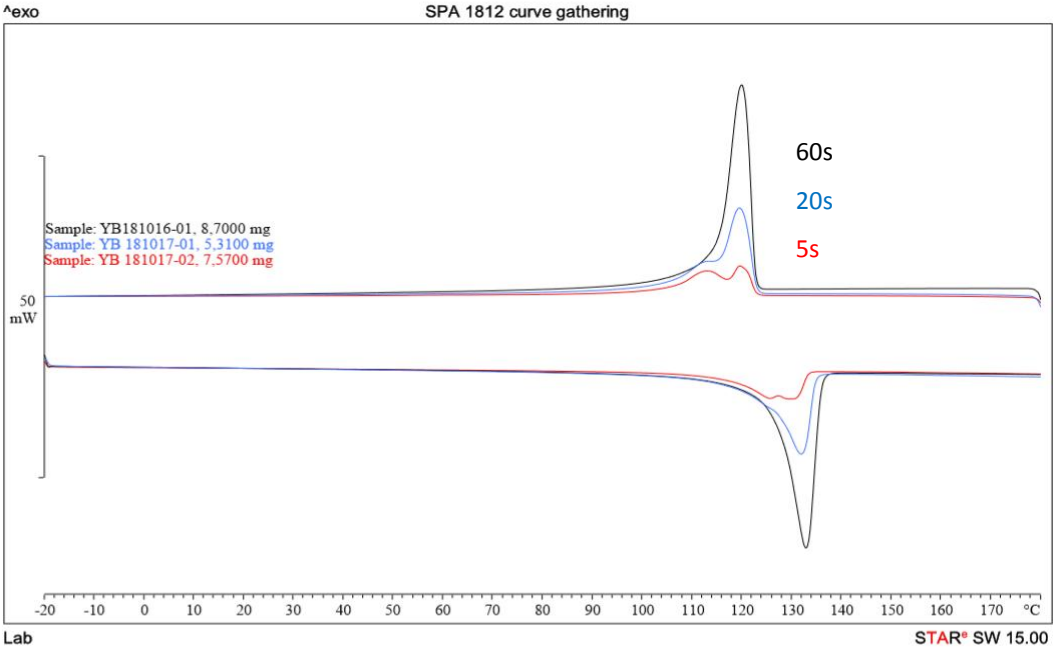

Figure 10: DSC profiles of the crystallization and the second melting of homopolymers produced with CpZ at short reaction times.

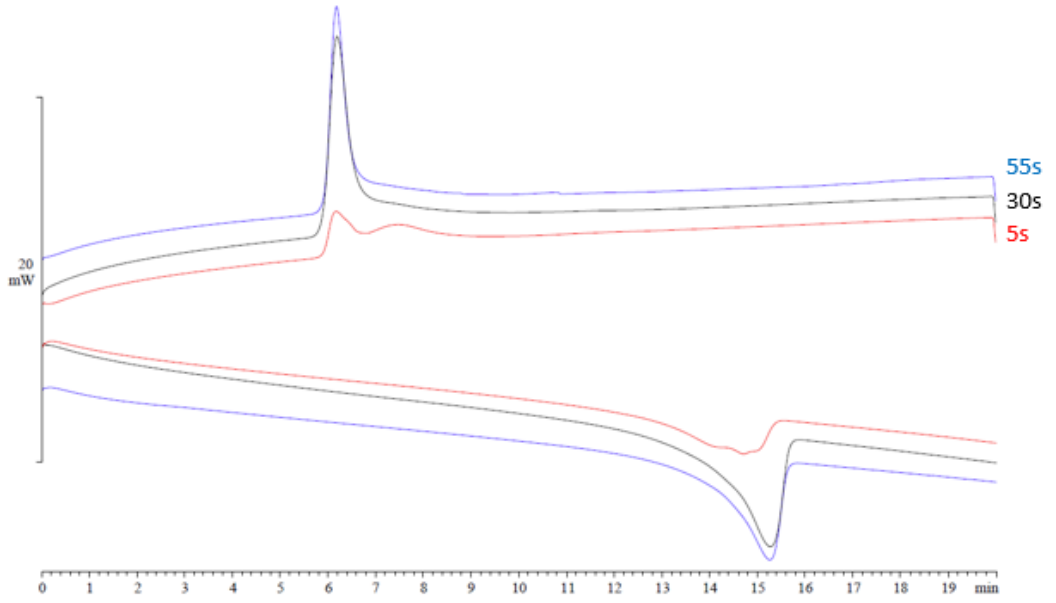

Figure 11: Evolution of thermal properties for classic metallocene CpZ. Reaction conditions: C_2 + 8 wt % 1-C_6 in gas feed.

5 Conclusions

A novel stopped-flow reactor with annular geometry has been developed to study the nascent stages of olefin polymerization in the gas phase. The new reactor can be used to perform

polymerization reactions over a wide range of operating conditions that allow to expose the catalyst and growing polymer particles to heat and mass transfers that are representative of those reached in industrial reactors, making it a valuable tool for the study of the nascent phase of polymerization. The associated software tool allows one to estimate the rate of reaction in-line without the need for additional sampling, and to build a rate curve without needing to run several different experiments as was previously the case.

The ASFR was used to help explain the poor performance of a commercial catalyst in a laboratory scale reactor where it is not possible to do very short reactions and to follow the thermal characteristics of the process gases flowing over the particles. It was observed that the catalyst that seemed to perform poorly actually activated much more rapidly than the reference catalyst, and generated significant amounts of heat, resulting in its own thermal deactivation. And finally, it was also possible to distinguish the time to fragmentation for homo- and copolymers on the same support. It was seen that the support seemed to fragment more quickly in the case of the copolymerization experiment, undoubtedly due to the more rapid accumulation of polymer in the pores of the particle.

It should be underlined that while this tool can indeed provide insight into catalyst behaviour, and eventually the short time evolution of particle morphology and polymer properties, it is not able to completely mimic reaction conditions in a real commercial gas phase reactor. As stated above the hydrodynamics and residence time distribution of a fluidized bed reactor are very different from what we have here, and are of course scale dependent. Nevertheless, the ASFR is capable of allowing us to look at the impact of relative velocities, gas phase composition, catalyst loading on the short time rates of polymerization, material properties, and evolution of particle morphology in realistic situations in ways that cannot be done with other more conventional reactors.

6 Nomenclature

Symbols:

C_p: Heat capacity of the fixed bed (J/kg/K)

C_{p_c}: Heat capacity of the catalyst (J/kg/K)

C_{pg}: Heat capacity of the gas (1714 J/kg/K)

$C_{p_{\mathrm{glassWool}}}$: Heat capacity of the glass wool (840 J/kg/K)

$C_{p_{\mathrm{PE}}}$: heat capacity of the polymer (2150 J/kg/K)

$C_{p_{\mathrm{s}}}$: heat capacity of the salt (890 J/kg/K)

d_{p}: the particle diameter (the salt diameter was used) (45×10^{-6} m)

d_{R}: Bed diameter ($d_{\mathrm{R}} = d_{\mathrm{R}}^{\mathrm{out}} - d_{\mathrm{R}}^{\mathrm{in}}$ = 5.7 mm) (m)

$d_{\mathrm{R}}^{\mathrm{out}}$: Diameter of the external bed cylinder (0.01478 m)

$d_{\mathrm{R}}^{\mathrm{in}}$: Diameter of the internal bed cylinder (or membrane) (0.009 m)

F_{g}: Mass flow rate of the gas (kg/s)

h_{w}: Heat transfer coefficient at the reactor internal-side wall (between the gas and the external wall) (W/m²/K)

$(h_{\mathrm{w}})_0$: stagnant/ conductive contribution to h_{w} (W/m²/K)

$(h_{\mathrm{w}})_{\mathrm{t}}$: turbulent/convective contribution to h_{w} (W/m²/K)

k_{g}: thermal conductivity of the monomer gas (0.0294 W/m/K)

k_{s}: thermal conductivity of the salt (1.15 W/m/K)

m: mass of the fixed bed (kg)

m_{c} : mass of the catalyst (kg)

$m_{\mathrm{glassWool}}$: mass capacity of the glass wool (kg)

m_{PE}: mass of polymer (kg)

m_s: mass of the salt (kg)

Re: Reynolds number (-)

R_{p}: Reaction rate (kg/s)

$R_{\mathrm{p,c}}$: Reaction rate per catalyst mass, or activity, (g PE/g cat/h)

Q_{r}: Total heat of polymerization (W)

$\hat{Q}_{\mathrm{r}}$: Estimated heat of the reaction (W)

S_{w}: Heat transfer surface area of the walls of the annular space (m²)

T: Fixed bed temperature (gas and solid) (K)

$\hat{T}$: Estimated bed temperature (K)

$T_{\mathrm{g}}^{\mathrm{in}}$: Inlet gas temperature (K)

T_{oven}: Oven temperature (K)

T_{w}: Temperature of the walls of the external annular space (K)

V: Volume of the fixed bed (m^3)

X_i: Factors in the factorial design

Y: Yield of polyethylene (g)

Greek letters

β: parameter in heat transfer coefficient equation (β=1 in Kunii and Levenspiel)

γ: parameter in heat transfer coefficient equation ($\gamma = 2/3$ in Kunii and Levenspiel)

ΔH_{p}: the enthalpy of polymerization (3830×10^3 J/kg)

ε: Porosity of the fixed bed (m^3 void / m^3 bed)

θ: Tuning parameter of the estimator (-)

ρ_{g}: Density of the gas (kg/m^3)

φ_{w}: A dimensionless number in heat transfer coefficient equation (-)

Abbreviations:

ASFRp: Annular stopped flow reactor prototype

ASFR: Annular stopped flow reactor

CGC: A constrained geometry metallocene catalyst

CpZ: Zirconocene catalyst

CR: Cylindrical disc-shaped reactor

DOE: Design of experiments

HDPE: High density polyethylene

LDPE: Linear density polyethylene

PE: Polyethylene

SFR: Stopped flow reactor

TEA: Triethyl aluminum

TIBA: Triisobutylaluminum

ZN: Ziegler-Natta catalyst

7 References

[1] J. B. P. Soares, T. F. L. McKenna, *Polyolefin reaction engineering*, Wiley-VCH, Weinheim, **2012**.

[2] T. F. L. McKenna, *Macromolecular Reaction Engineering* **2019**, *13*, 1800026.

[3] US7696289B2, invs.: D. Brett Fischbuch, Robert O. Hagerty, Sandy C. Hinds, Douglas R. Holroyd, Ai Vey Ng, Diwaker Singh.

[4] S. Floyd, K. Y. Choi, T. W. Taylor, W. H. Ray, *J. Appl. Polym. Sci.* **1986**, *32*, 2935.

[5] S. Floyd, K. Y. Choi, T. W. Taylor, W. H. Ray, *J. Appl. Polym. Sci.* **1986**, *31*, 2231.
[6] E. Tioni, R. Spitz, J. P. Broyer, V. Monteil, T. McKenna, *AIChE J.* **2012**, *58*, 256.
[7] T. F. McKenna, J. B. P. Soares, *Chemical Engineering Science* **2001**, *56*, 3931.
[8] T. F. L. McKenna, A. Di Martino, G. Weickert, J. B. P. Soares, *Macromolecular Reaction Engineering* **2010**, *4*, 40.
[9] T. F. L. McKenna, M. A. Bashir, "Fragmentation, Particle Growth and Single Particle Modelling," *Multimodal Polymers with Supported Catalysts*, A. R. Albunia, F. Prades, D. Jeremic, Eds., Springer International Publishing, Cham **2019**, p. 81.
[10] T. F. L. McKenna, E. Tioni, M. M. Ranieri, A. Alizadeh, C. Boisson, V. Monteil, *Can. J. Chem. Eng.* **2013**, *91*, 669.
[11] V. Busico, R. Cipullo, V. Esposito, *Macromol. Rapid Commun.* **1999**, *20*, 116.
[12] B. Liu, H. Matsuoka, M. Terano, *Macromol. Rapid Commun.* **2001**, *22*, 1.
[13] A. Di Martino, J.-P. Broyer, D. Schweich, C. de Bellefon, G. Weickert, T. F. L. McKenna, *Macromol. React. Eng.* **2007**, *1*, 284.
[14] T. Taniike, V. Q. Thang, N. T. Binh, Y. Hiraoka, T. Uozumi, M. Terano, *Macromol. Chem. Phys.* **2011**, *212*, 723.
[15] A. Di Martino, J. P. Broyer, R. Spitz, G. Weickert, T. F. McKenna, *Macromol. Rapid Commun.* **2005**, *26*, 215.
[16] A. Di Martino, G. Weickert, T. F. L. McKenna, *Macromol. React. Eng.* **2007**, *1*, 165.
[17] A. Di Martino, G. Weickert, T. F. L. McKenna, *Macromol. React. Eng.* **2007**, *1*, 229.
[18] F. M. Silva, J. P. Broyer, C. Novat, E. L. Lima, J. C. Pinto, T. F. McKenna, *Macromol. Rapid Commun.* **2005**, *26*, 1846.
[19] B. Olalla, J.-P. Broyer, T. F. L. McKenna, *Macromol. Symp.* **2008**, *271*, 1.
[20] B. Browning, I. Pitault, N. Sheibat-Othman, E. Tioni, V. Monteil, T. F. L. McKenna, *Chemical Engineering Journal* **2012**, *207–208*, 635.
[21] B. Browning, N. Sheibat-Othman, I. Pitault, T. F. L. McKenna, *AIChE J.* **2014**, *60*, 3511.
[22] E. Tioni, V. Monteil, T. McKenna, *Macromolecules* **2013**, *46*, 335.
[23] G. Soave, *Chemical Engineering Science* **1972**, *27*, 1197.
[24] G. E. P. Box, J. S. Hunter, W. G. Hunter, *Statistics for experimenters: Design, innovation, and discovery*, 2nd edition, Wiley, **2005**.
[25] M. A. Al-Juaied, D. Lafarga, A. Varma, *Chemical Engineering Science* **2001**, *56*, 395.
[26] J. G. McCarty, *Catalysis Today* **1995**, *26*, 283.
[27] A. Beretta, P. Baiardi, D. Prina, P. Forzatti, *Chemical Engineering Science* **1999**, *54*, 765.
[28] G. Groppi, W. Ibashi, E. Tronconi, P. Forzatti, *Chemical Engineering Journal* **2001**, *82*, 57.
[29] G. Groppi, W. Ibashi, M. Valentini, P. Forzatti, *Chemical Engineering Science* **2001**, *56*, 831.
[30] V. Specchia, G. Baldi, S. Sicardi, *Chemical Engineering Communications* **1980**, *4*, 361.
[31] D. Kunii, O. Levenspiel, *Fluidization Engineering (Series in Chemical Engineering)*, **1991**.
[32] J. Gauthier, G. Bornard, *IEEE Transactions on Automatic Control* **1981**, *26*, 922.
[33] J. P. Gauthier, H. Hammouri, S. Othman, A Simple Observer for Nonlinear Systems Applications to Bioreactors **1992**.
[34] N. Othman, T. F. Mckenna, A. M. Santos, G. Févotte, *The Canadian Journal of Chemical Engineering* **2002**, *80*, 88.
[35] A. D. Martino, G. Weickert, T. F. L. McKenna, *Macromolecular Reaction Engineering* **2007**, *1*, 165.